JGR Oceans

RESEARCH ARTICLE
10.1029/2019JC015876

Do Beach Profiles Under Nonbreaking Waves Minimize Energy Dissipation?

S. Maldonado[1]

[1]Faculty of Engineering and Physical Sciences, University of Southampton, Southampton, UK

Key Points:
- We revisit and advance previous theoretical works on the shape adopted by equilibrium beach profiles
- Results suggest that profiles under nonbreaking waves tend to minimize wave energy dissipation
- This work may promote and aid future test of the energy minimization hypothesis for beach profiles and other geomorphological features

Correspondence to:
S. Maldonado,
s.maldonado@soton.ac.uk

Citation:
Maldonado, S. (2020). Do beach profiles under nonbreaking waves minimize energy dissipation? *Journal of Geophysical Research: Oceans*, *125*, e2019JC015876. https://doi.org/10.1029/2019JC015876

Received 15 NOV 2019
Accepted 9 APR 2020
Accepted article online 16 APR 2020

Abstract The hypothesis that equilibrium beach profiles under nonbreaking waves minimize wave energy dissipation was considered by Larson et al. (1999 *Coast. Eng.* **36** 59-85). Larson et al. approached the hypothesis as a variational problem, assuming a priori that the solution (the extremal profile) followed a power law with a freely tunable exponent, which was varied so as to extremize the relevant functional. Here, we revisit this hypothesis and solve the associated variational problem approximately via analytical means, without a priori assumptions on the mathematical structure of the solution. We remark that for the solution to be realistic, the problem formulation must consider additional constraints; for example, the bed slope angle must not exceed the sediment's angle of repose. Incidentally, the solution we derive recovers the power law prescribed by Larson et al., which is in turn backed by a large body of empirical evidence. However, the exponent of the power in our solution is not an arbitrarily free parameter; it depends on the parametrization of the bed shear stress (the main mechanism by which nonbreaking waves dissipate energy), and predicted values of the exponent are supported by previous research. The power law curve derived here agrees well with empirical data from field and laboratory, suggesting that a principle of energy economy may indeed underpin the particular shape adopted by beach profiles under nonbreaking waves. This theoretical study aims at promoting and aiding further tests of this hypothesis.

Plain Language Summary Beach profiles describe the sea's depth as a function of the distance from the shore. Waves sculpt the beach profile as they propagate, dissipating energy in the process; nonbreaking waves do so almost exclusively via friction with the seabed. From decades of data collection, it is well known that in equilibrium profiles the depth varies with the distance offshore according to a power law, but the reason for this is much less understood. In this paper, we revisit and advance previous research in order to prove theoretically that the reason may lie behind a principle of energy economy (found ubiquitously throughout nature). In particular, nonbreaking waves appear to sculpt beach profiles into equilibrium shapes that tend to minimize the energy being thereafter dissipated by the waves themselves.

1. Introduction

Beach profiles describe the variation of the water depth, h, with cross-shore distance, x (see Figure 1). Due to their central role in determining the hydro-morphodynamics of coastal areas, equilibrium beach profiles (EBPs) represent key concepts commonly employed by Earth scientists and coastal engineers, particularly when utilizing reduced-order models. For example, researchers and engineers may prescribe theoretical EBPs to models employed to design beach nourishments (Dean, 2003); predict the evolution of the shoreline (Jara et al., 2015), including its response to sea level rise (Dean & Houston, 2016) and the emergence of large-scale coastline forms (Ashton & Murray, 2006; Falqués & Calvete, 2005); or assess the coastal protection provided by vegetation (Guannel et al., 2015). It is common to treat the relation between h and x as one obeying a power law, that is, $h \sim x^{m_p}$, where the exponent m_p is usually obtained either via curve fits to empirical data, some physics-based considerations, or a combination of both. Good reviews on EBPs, along with discussions on the underlying assumptions of different approaches, can be found in, for example, Dean (1991), Inman et al. (1993), and Larson et al. (1999). Since we are solely concerned with beach profiles in equilibrium state, understood as those which are attained after the seabed has been subject to steady (e.g., monochromatic) wave forcing for a sufficiently long time, the word "equilibrium" may be here dropped for convenience.

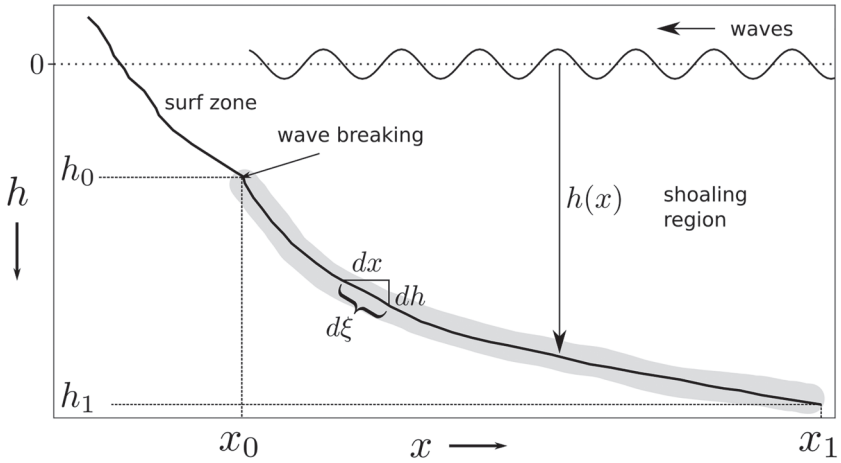

Figure 1. Sketch of the problem illustrating a typical beach profile where two distinct regions can be identified, separated by the wave breaking point/bar. We are concerned with the outer part of the profile subject to shoaling, nonbreaking waves (highlighted in gray).

Our focus is on the energy-dissipation-based theories used to explain the specific shape, or function $h(x)$, that EBPs adopt. For mass-balance-based approaches, such as that by Bowen (1980), see the reviews recommended above; for a nonphysics-based derivation, see, for example, Dong (2008), who uses information theory. Probably the best-known energy-dissipation-based approach is that followed by Dean (1977), building on Brunn (1954), who considered two cases, namely, that the rate of wave energy dissipation is uniform (along x) either when previously divided per i) unit volume of water or ii) unit bed area. In both cases, the power law is recovered, obtaining values of the exponents of $m_p = 2/3$ and $m_p = 2/5$, respectively. Perhaps a less-known energy-dissipation-based assumption adopted to explain EBPs is that by Larson et al. (1999), who posed the hypothesis that in EBPs under nonbreaking waves, the total rate of wave energy dissipation per unit beach width and time attains a minimum. In other words, that the beach attains an equilibirum shape such that the waves propagating across the shoaling part of the profile minimize the energy they lose due to bed friction. Following a variational approach, Larson et al. (1999) use linear wave theory to formulate a functional associated with energy dissipation $J[h(x)]$, for which a minimum is sought. Larson et al. (1999) then assume, based on empirically derived knowledge, that the extremal function $h(x)$ follows a power law relation $h \sim x^{m_p}$, thus bypassing the solution to the associated Euler-Lagrange equation (which must be satisfied if J is to attain an extremum at h) and varying m_p so as to extremize $J[h]$, subject to two given boundary conditions (i.e., the depths at two given locations in the profile). Following a similar, albeit ultimately opposed, line of reasoning, Jenkins and Inman (2006) invoke the maximum entropy production formulation of the second law of thermodynamics and treat the shorezone system as one that *maximizes* the waves' energy dissipation (the exact opposite of Larson et al., 1999). Then, Jenkins and Inman (2006) claim that an EBP described by an elliptic cycloid satisfies this condition. However, in the appendix paper (Maldonado & Uchasara, 2019), we argue that the solution proposed by Jenkins and Inman (2006) ought to be scrutinized further, a proposition that has recently been supported by Faraoni (2019), based in turn on the work by Chen et al. (2015).

In this paper, we revisit the hypothesis posed by Larson et al. (1999) regarding the minimization of energy dissipation in profiles under nonbreaking waves. The main motivation to do so is that, unlike the assumptions adopted by Dean (1977) and Brunn (1954), extremization of physical quantities such as energy is a principle that holds certain universality (indeed, variational principles underpin Lagrangian and Hamiltonian mechanics, which are in turn foundational for both classical and modern physics). If shown to be correct, the energy minimization hypothesis may in future be tested for other geomorphological features besides beach profiles. Instead of assuming a form of the extremal function a priori (i.e., that $h \sim x^{m_p}$, as do Larson et al., 1999), we attempt to solve the variational problem directly. We show that the problem formulation must state additional constraints grounded on evidence-based considerations for the solution to be realistic. The analytical solution we propose to the constrained variational problem is approximate, but its satisfactory validation against empirical data backs the argument that EBPs do tend to minimize the dissipation of energy of nonbreaking waves. Some derivations presented here may be considered textbook

knowledge or repetitions of those found in referenced works, but one objective of this manuscript is to complement the derivations in previous publications on this topic for the sake of straightforward reproducibility and further testing of this theory. The study neglects the nearshore part of the profile (or surf zone) because the morphology of this region is well described by the $h \sim x^{2/3}$ profile (Brunn, 1954; Dean, 1977; Fredsøe & Deigaard, 1992; Larson et al., 1999), and its underlying assumption of uniform energy dissipation per unit volume of water is justifiable (Fredsøe & Deigaard, 1992; Wang & Kraus, 2005).

The manuscript is structured as follows. The problem is formulated in section 2, and a preliminary (unconstrained) solution is derived in section 3. In section 4, the constraints are incorporated into the preliminary solution, which is then further analyzed based on its physical meaningfulness and compared against empirical data. The main strengths and limitations of the present work are discussed in section 5, and some final remarks are presented in section 6.

2. Problem Formulation

We seek a theoretical beach profile, or function $h(x)$, that minimizes the rate of energy dissipation of nonbreaking waves, subject to known boundary conditions, namely, the positions and values of two given depths: $h(x_0) = h_0$ and $h(x_1) = h_1$ (see Figure 1). Additionally, for any solution to be physically meaningful, the following features common to natural beach profiles must be reproduced:

a. The local bed slope angle cannot exceed the sediment's angle of repose, ϕ, that is, $|h'(x)| \leq \tan\phi$ for all $x \in [x_0, x_1]$, where $h'(x) \equiv dh(x)/dx$.
b. The water depth increases monotonically with cross-shore distance, that is, $h(x)$ is a strictly increasing function.
c. The increase of h with x is "smooth." For our purposes, it is sufficient to require that the second derivative of h (i.e., h'') is small everywhere in the interval $x \in [x_0, x_1]$.
d. The beach profile is concave upward near the wave breaking point and tends to a smaller, constant value offshore, that is, $|h'(x_1)| < |h'(x_0)|$ and $h''(x \to x_1) \to 0$ (the concave nature of h near x_0 may be verified qualitatively).

Furthermore, the following assumptions pertaining to the study area are invoked:

1. Straight shoreline with normally incident, monochromatic waves of small, constant amplitude.
2. The shallow water approximation of linear wave theory is assumed valid.
3. The analysis is limited to shoaling (nonbreaking) waves.
4. Variations of the local water depth due to long-period oscillations such as tides are neglected.
5. The beach is composed of uniform, erodible, impermeable sediment.

A 1D profile is considered (see Figure 1), where h varies exclusively with x, measured from some conveniently chosen origin. Note that h is measured positively downwards from a given datum (e.g., the mean sea level), which is time independent as per Assumption 4. Since we consider nonbreaking, inviscid waves, energy dissipation must occur exclusively at the bottom boundary layer. Our first objective is to express this energy dissipation, averaged over a wave period, as a function of h, as described next.

The instantaneous rate of energy dissipation of a column of water, under the influence of surface waves, per unit bed area, $\epsilon(t)$ (where t is time), may be expressed as the product of the bed shear stress, $\tau_b(t)$, and the near-bed flow velocity, $u_b(t)$, that is, $\epsilon(t) = \tau_b(t)u_b(t)$. The magnitude of the bed shear stress is typically parameterized according to $|\tau_b| \propto u_b^2$, such that the rate of energy dissipation averaged over a wave period (denoted by the overbar) per unit bed area follows the trend $\bar{\epsilon} \sim u_{bo}^3$ (see, e.g., Svendsen, 2006), where u_{bo} is the amplitude or maximum value of $u_b(t)$. However, the proportionality coefficient in $|\tau_b| \propto u_b^2$ may ultimately depend (via the friction coefficient) on u_b in some complex manner, for example, as an empirically derived function of the wave Reynolds number (see Appendix A). Since we seek to establish an expression of the form $\bar{\epsilon}(h)$, and noting that linear wave theory allows us to write u_{bo} in terms of h (see Appendix B), we further assume (as do, e.g., Jenkins & Inman, 2006) that there is some real, positive constant n_τ, such that the bed shear stress may be cast in the form $|\tau_b| = K_\tau |u_b|^{n_\tau}$, where K_τ must be independent of both u_b and h. Consequently, the rate of energy dissipation, $\bar{\epsilon}$, goes like $u_{bo}^{(n_\tau+1)}$, with n_τ expected to lie in the range $1 \leq n_\tau \leq 2$ (Appendix A).

From the theory of linear waves in shallow water, we know (Appendix B) that $u_{bo} \sim H(x)h^{-1/2}$, where $H(x)$ is the local wave height, which in the absence of refraction (Assumption 1 but see section 5),

varies across the profile due to shoaling as $H \sim h^{-1/4}$, leading to $u_{bo} \sim h^{-3/4}$. Therefore, the local wave-period-average dissipation rate per unit area of bed varies as

$$\bar{\epsilon} \sim u_{bo}^{(n_\tau+1)} \sim h^{-\frac{3}{4}(n_\tau+1)}. \tag{1}$$

To simplify future treatment, we collect all relevant terms that are independent of h into a term K_ϵ and define $n_\epsilon \equiv \frac{3}{4}(n_\tau + 1)$, such that

$$\bar{\epsilon} = K_\epsilon h^{-n_\epsilon}. \tag{2}$$

Turning now to the study region (the shoaling part of the profile), consider a water volume V of arbitrary thickness B in the longshore direction, delimited in the vertical by the free surface and the seabed and in the cross-shore direction by the planes $x = x_0$ and $x = x_1$ (see Figure 1). Recalling that $\bar{\epsilon}$ is expressed per unit bed area and noting that a small strip of bed area at the boundary of the volume of interest is given by $Bd\xi = B\sqrt{dx^2 + dh^2} = B\sqrt{1 + (dh/dx)^2}dx$, the total rate of energy dissipation (per wave period) in the volume considered is

$$\mathcal{D} = BK_\epsilon \int_{x_0}^{x_1} h^{-n_\epsilon} \sqrt{1 + \left(\frac{dh}{dx}\right)^2}\, dx. \tag{3}$$

Thus, as in Larson et al. (1999), the problem reduces to finding the function $h(x)$ that minimizes the above integral, subject to known boundary conditions. But unlike Larson et al. (1999), we further require that $h(x)$ satisfies conditions a–d discussed at the beginning of this section.

3. Preliminary (Unconstrained) Solution

From equation (3), the functional to be extremized is

$$J[h(x)] = \int_{x_0}^{x_1} h^{-n_\epsilon} \sqrt{1 + (h')^2}\, dx. \tag{4}$$

However, for convenience and on account of $h(x)$ being a monotonic function (condition b in section 2), we will find the inverse function $x(h)$ and rewrite the functional for which we seek a minimum as

$$J[x(h)] = \int_{h_0}^{h_1} L\left[x(h), x'(h); h\right] dh, \tag{5}$$

where $x' \equiv dx/dh$ and $L\left[x(h), x'(h); h\right] = h^{-n_\epsilon}\sqrt{1 + (x')^2}$. A necessary condition for $J[x]$ to attain an extremum, which we presume to be a minimum, at $x(h)$ is that the Euler-Lagrange equation,

$$\frac{d}{dh}\frac{\partial L}{\partial x'} - \frac{\partial L}{\partial x} = 0, \tag{6}$$

be satisfied. Noting that $\partial L/\partial x = 0$, a first integration with respect to h yields $\partial L/\partial x' = h^{-n_\epsilon}[1 + (x')^2]^{-1/2}x' =$ const., which can be rearranged to give $dx/dh = \sqrt{\alpha h^{2n_\epsilon}/(1 - \alpha h^{2n_\epsilon})}$, where α is a constant associated with the integration. Separation of variables prior to a second integration then yields

$$x = \int \sqrt{\frac{\alpha h^m}{1 - \alpha h^m}}\, dh + \beta', \tag{7}$$

where β' is a second integration constant and $m \equiv 2n_\epsilon$. It should be noted that equation (7) is essentially the same expression to which both Jenkins and Inman (2006) and Larson et al. (1999) arrive in their respective derivations. However, as discussed in section 1, the latter ultimately ignore it (i.e., they assume instead that $h(x)$ follows a power law), whereas the former propose a solution that invites further scrutiny (Maldonado & Uchasara, 2019).

Solution to the integral in equation (7) for otherwise arbitrary positive values of m can be found with the aid of Wolfram Mathematica in terms of the Gaussian hypergeometric function ${}_2F_1$, namely,

$$\int \sqrt{\frac{\alpha h^m}{1 - \alpha h^m}}\, dh = \frac{2h\sqrt{\alpha h^m}}{2 + m}\, {}_2F_1\left(\frac{1}{2}, \frac{1}{2} + \frac{1}{m}; \frac{3}{2} + \frac{1}{m}; \alpha h^m\right) + \beta, \tag{8}$$

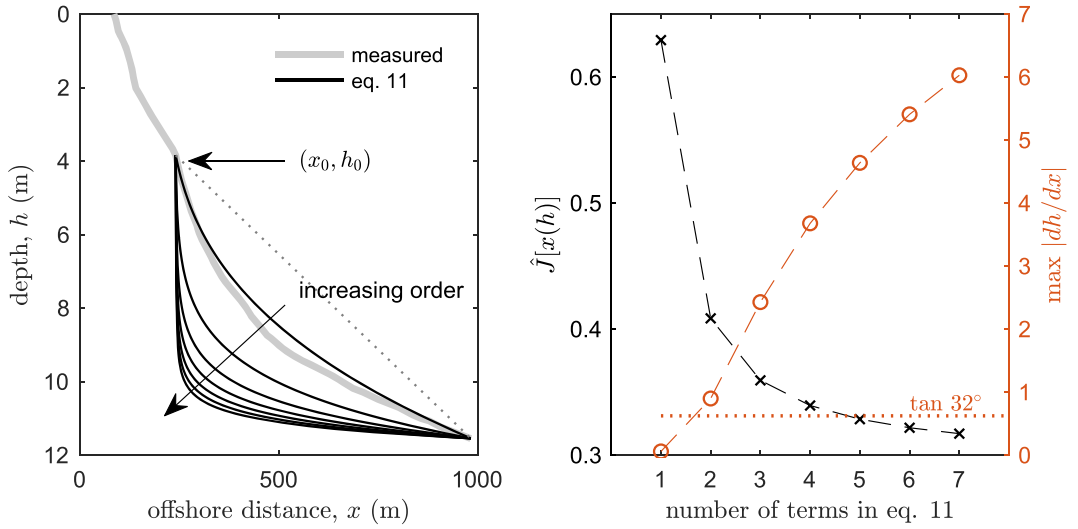

Figure 2. Increasing the order (i.e., retaining more terms in the series, in this case up to seven) of the preliminary solution (11) tends to minimize $J[x]$ (equation 5) by increasing h in general (for all x), at the cost of unrealistically steep bed slopes near x_0. Left: An illustration of the profiles predicted by equation (11) as the order of the solution increases; a linear profile (dotted line) is added for reference. Right (left y-axis): Normalized functional $\hat{J}[x(h)]$, defined as the ratio $J[x(h)]/J[\text{linear profile}]$, yielded by equation (11) as a function of the number of terms retained in the series. Right (right y-axis): Maximum local bed slope for the predicted profile (always attained at x_0) as a function of the number of terms retained in equation (11). The measured profile is J&I b.

where β is an integration constant and the hypergeometric function ${}_2F_1(a, b; c; z)$ is given by the series expansion

$$ {}_2F_1(a, b; c; z) = \sum_{n=0}^{\infty} \frac{(a)_n (b)_n}{(c)_n} \frac{z^n}{n!}, \tag{9} $$

where the (rising) Pochhammer symbol $(q)_n$ is defined as

$$ (q)_n = \begin{cases} 1 & n = 0 \\ q(q+1) \ \ldots \ (q+n+1) & n > 0. \end{cases} \tag{10} $$

As an illustration, we write below the solution to equation (7) by retaining solely the first four terms of the series:

$$ x(h) = \frac{2h\sqrt{\alpha h^m}}{2+m} \left[1 + \frac{\left(\frac{1}{2}\right)_1 \left(\frac{1}{2}+\frac{1}{m}\right)_1}{\left(\frac{3}{2}+\frac{1}{m}\right)_1} \alpha h^m + \frac{\left(\frac{1}{2}\right)_2 \left(\frac{1}{2}+\frac{1}{m}\right)_2}{\left(\frac{3}{2}+\frac{1}{m}\right)_2} \frac{\alpha^2 h^{2m}}{2} + \frac{\left(\frac{1}{2}\right)_3 \left(\frac{1}{2}+\frac{1}{m}\right)_3}{\left(\frac{3}{2}+\frac{1}{m}\right)_3} \frac{\alpha^3 h^{3m}}{6} + \ldots \right] + \beta, \tag{11} $$

where the constants α and β are obtained from the boundary conditions.

The integral in equation (7) may also be solved via Taylor series expansion of the integrand. However, this alternative presents some limitations when compared to equation (11), as discussed in Appendix C.

3.1. Boundary Conditions

Incorporation of the boundary conditions $x(h = h_0) = x_0$ and $x(h = h_1) = x_1$ into the preliminary solution (11) yields, for a finite number of terms retained, a system of two nonlinear equations for the two unknowns, α and β. Solutions are found numerically. For selection of the shoreward boundary (x_0, h_0) in a given beach profile, we look for the wave breaking point, identified as a point of abrupt change in the bed slope in the direction of the propagating waves. There is little ambiguity in the selection of this point (see, e.g., Figures 1, 2, or 3). However, the same cannot be said about the seaward boundary (x_1, h_1), as also pointed out by Larson

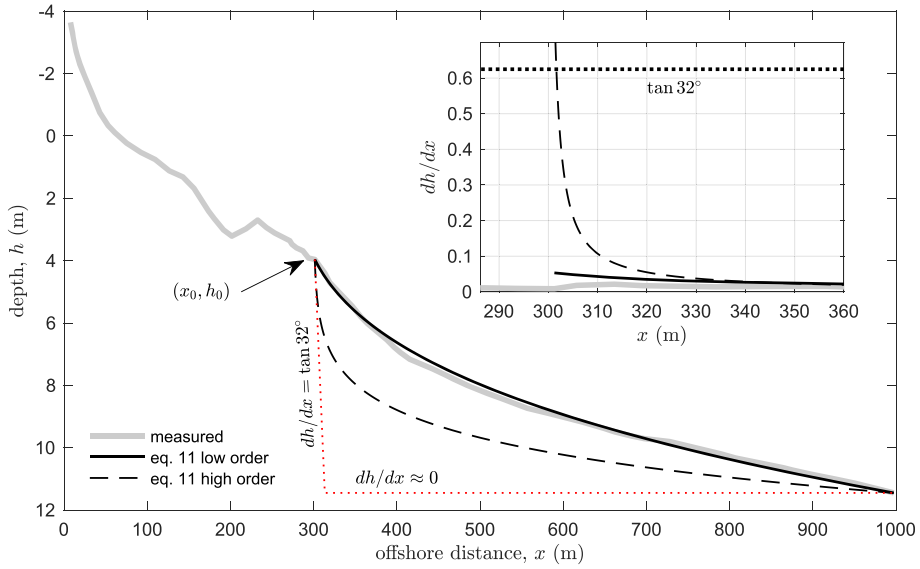

Figure 3. Comparison between the highest-order solution that complies with the constraint $|h'(x)| \leq \tan\phi$ for all $x \in [x_0, x_1]$ (see subplot) and the next higher-order solution that violates this constraint. The former (latter) is referred to as "low order" ("high order") solution. An unrealistic profile (red dotted line) is added for future reference in the text (section 5). The measured profile is J&I e, which is representative of all other profiles considered.

et al. (1999). Typical profiles tend to a uniform bed slope away from the shore (condition d; see any figure in this paper) up to a point where waves stop interacting, from a morphodynamic perspective, with the seabed (sometimes referred to as the closure depth). In principle, any point along this constant-slope part of the profile could be used as seaward boundary condition. In section 4.4 we explore the solution's sensitivity to the selection of (x_1, h_1). Also, in section 5 we discuss an alternative boundary condition, based on h' at $x = x_0$, that was tested unsuccessfully.

4. The Solution and Results

In this section, we incorporate constraints a–d into the preliminary solution prior to comparing it against field and laboratory data (described in section 4.1). Sensitivity of the constraints-complying solution to the selection of the seaward boundary condition and the physical parameter n_τ is analyzed in sections 4.4 and 4.5, respectively. The predictive performance of the proposed solution is contrasted against that of best-fit power law curves in section 4.6.

4.1. Data Employed for Comparison

In order to test the energy minimization hypothesis, the theoretical profile derived from variational considerations is compared against data from both laboratory and field. For field data, we select the six profiles shown in Figure 8 of Jenkins and Inman (2006) (labeled here J&I a, J&I b, … , J&I f), which were measured during a 6-year period near Oceanside, California. These profiles have been selected because the analytical treatment carried out by Jenkins and Inman (2006), who used these profiles for validation, builds on similar assumptions to those adopted here, and because in all of these profiles the limit of the surf zone (point x_0) can be readily identified. For laboratory profiles, we employ a subset of those reported in Wang and Kraus (2005), which were measured in a large tank specifically designed to minimize scale-related distortions and focus on beach response to cross-shore sediment transport, thus complying with the 1D assumption underpinning the analysis presented here. Solely final profiles (described in Table 1 and shown in Figure 1 of Wang & Kraus, 2005) with "Run ID" ending in 209, 270, and 559 (we label these profiles W&K 209, W&K 270, and W&K 559) are utilized based on the amplitude of the waves employed during their corresponding experiments; we have selected the smallest amplitudes, in keeping with Assumption 1 in section 2.

4.2. Incorporation of Constraints

A posteriori, it is observed (see below) that the unconstrained solution (11) complies naturally with conditions b–d, but not necessarily with condition a (i.e., the "angle of repose" constraint: $|h'(x)| \leq \tan\phi$), to which we therefore devote our attention here. To the best of the author's knowledge, a variational problem

Table 1
Ratio of the Functional J[x(h)] (Equation 5) Obtained by Each Solution (Left Column) to That Arising From a Linear Profile (i.e., The Normalized Functional $\hat{J}[x]$ Shown in Figure 2)

	Jenkins and Inman						Wang and Kraus		
	a	b	c	d	e	f	209	279	559
equation 11 low order	0.53	0.63	0.58	0.42	0.65	0.49	0.66	0.71	0.52
equation 11 high order	0.32	0.41	0.36	0.24	0.43	0.29	0.45	0.51	0.34

Note. The "high order" solution yields smaller values of $J[x]$ than its "low order" counterpart. Both solutions yield smaller values of $J[x]$ than a linear profile.

with such a subsidiary condition (i.e., an inequality) cannot be solved exactly via standard analytical methods (see, e.g., Bronshtein et al., 2007; Cline, 2017; Courant & Hilbert, 1953, and section 5 for a discussion on this). Hence, a simple approach based on a posteriori knowledge on the behavior of the unconstrained solution is adopted, as discussed next.

Figure 2 shows that the effect of higher-order terms in the unconstrained solution is to increase the overall water depth h in the domain, which in turn tends to minimize the energy dissipation rate (or functional J; see Figure 2 right). This translates into steeper bed slopes near the boundary x_0, with the steepness of the slope also increasing with the order of the solutions. However, some of these bed slopes are physically unrealistic ($> \tan\phi$). Thus, we adopt a simple, heuristic approach to incorporate the angle of repose constraint, whereby highest-order terms in the solution are discarded one at a time until the condition $|h'(x)| \leq \tan\phi$ is satisfied for all $x \in [x_0, x_1]$. We use a standard value for sand of $\phi = 32° \Rightarrow \tan\phi = 0.625$ (Soulsby, 1997). Unless otherwise stated, $n_\tau = 2$ is assumed (i.e., $|\tau_b| = K_\tau u_b^2$), such that $n_\epsilon = 2.25 \Rightarrow m = 4.5$, but sensitivity to this parameter is explored in section 4.5.

Figure 3 compares, for a given profile, the highest-order solution that complies with $|h'(x)| \leq \tan\phi$ (referred to as "low order") against the next higher-order solution which violates this condition (labeled "high order"). Thus, the "high order" solution arising from equation (11) refers to that retaining the first two terms of the series, while the "low order" solution retains only the first term. The subplot in Figure 3 shows that the "high order" solution exceeds the angle of repose near the point x_0, while the "low order" solution complies with $|h'(x)| \leq \tan\phi$ for all $x \in [x_0, x_1]$. This is in agreement with Figure 2 (right). Both solutions predict a continuous, smooth bed slope (condition c) attaining a maximum at $x = x_0$ and asymptotically decreasing toward their value at x_1 (conditions b and d). For all the profiles considered in this study, the "high order" solution tends to minimize the value of the target functional at the cost of unrealistically steep bed slopes near x_0, as illustrated in Tables 1 and 2, which we discuss next.

Table 1 shows the value of the functional $J[x(h)]$ (equation 5) for each solution (estimated numerically), rendered nondimensional via division by $J[x(h) = \text{linear profile}]$ (i.e., the normalized functional $\hat{J}[x]$ shown in Figure 2). This table highlights two facts: i) the "high order" solution tends to minimize the functional for all profiles considered, as may be expected from inspection of Figure 2 and ii) all values are < 1, which means that an arbitrarily neighboring (but realistic) function $x(h)$ (in this case, a line) yields a larger value of $J[x]$. These two points, in combination with Figure 2, suggest that the stationary value to which the solution tends (as its order, and thus accuracy, increases) is indeed a minimum (or at the very least, cannot be a maximum; see section 5). Table 2 illustrates that in all cases considered, the "high order" solution violates the angle of repose constraint, while, conversely, the "low order" solution always complies with $|h'(x)| \leq 0.625$.

Table 2
Maximum Local Bed Slope Encountered at Some Point in the Profile Predicted by Each Solution; This Point is Always x_0

	Jenkins and Inman						Wang and Kraus		
	a	b	c	d	e	f	209	279	559
equation 11 low order	0.09	0.06	0.07	0.15	0.05	0.10	0.23	0.17	0.35
equation 11 high order	1.67	0.90	1.28	3.21	0.81	2.11	1.73	1.13	3.12

Note. The slope of repose ($\tan 32° = 0.625$) is exceeded in all cases by the "high order" solution but never by its "low order" counterpart. For reference, J&I (W&K) measured profiles present maximum local bed slopes of approximately 0.03 to 0.05 (0.2 to 0.4).

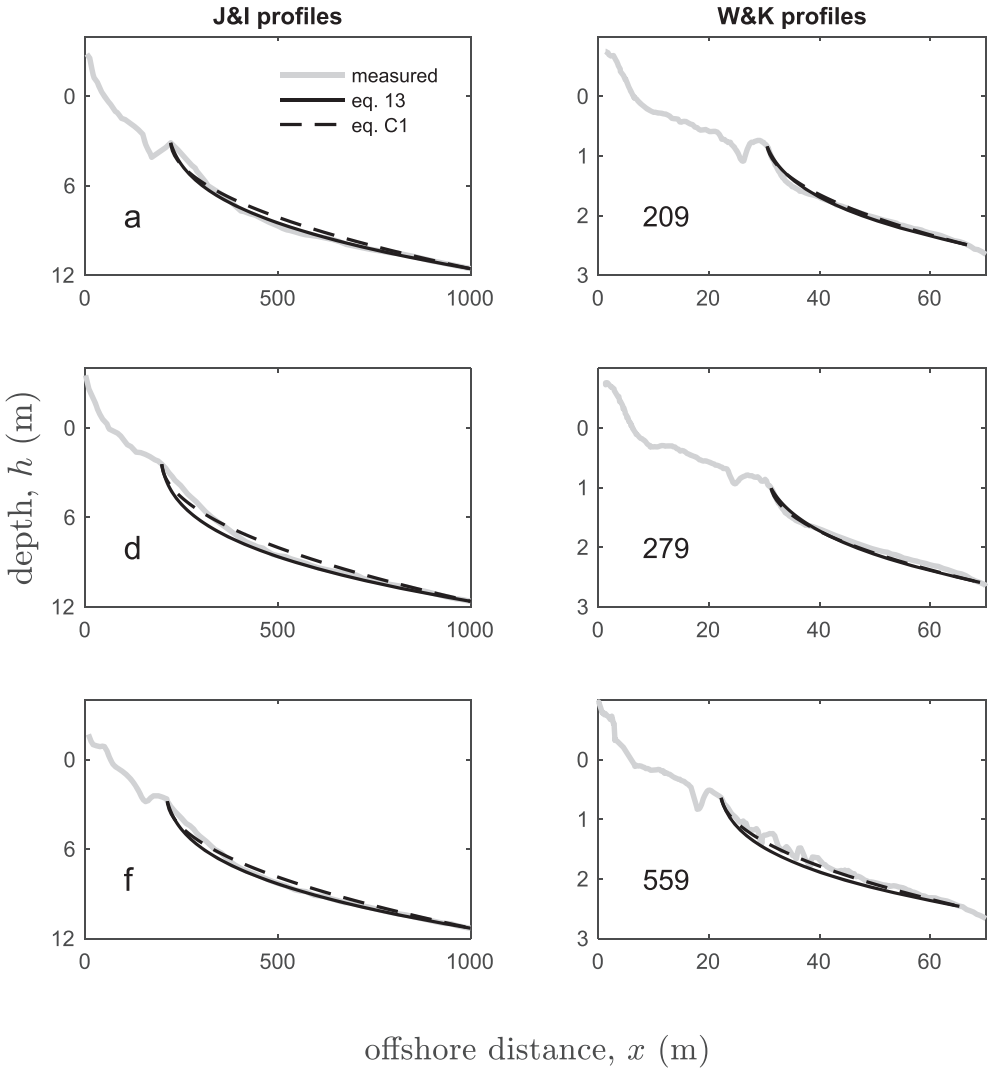

Figure 4. The proposed profile (equation 13) is compared against three profiles measured by Jenkins and Inman (2006) (left) and those by Wang and Kraus (2005) (right). Profiles by Jenkins and Inman (2006) not shown here can be found in other figures throughout the manuscript. Note that equation (13) is the same as "equation (11) low order" discussed in other parts of the paper. Equation C1 (dashed line) is discussed in Appendix C.

Moreover, the "low order" solution yields values of the maximum bed slopes which are comparable to those observed in the measured profiles.

Based on this analysis, we revisit the unconstrained solution derived in section 3 and propose a theoretical EBP that tends to minimize energy dissipation while complying with conditions a–d stated in section 2. This profile arises by retaining solely the first term of the series, namely,

$$x(h) = \frac{2\sqrt{\alpha}}{2+m} h^{\frac{2+m}{2}} + \beta, \tag{12}$$

which may be cast in the familiar power law form:

$$h(x) = \bar{\alpha}(x-\beta)^{\frac{4}{3n_\tau+7}}, \tag{13}$$

where $\bar{\alpha} = (2+m)^{\frac{2}{2+m}}(2\sqrt{\alpha})^{-\frac{2}{2+m}}$; recall that $m = 2n_\epsilon = \frac{3}{2}(n_\tau+1)$. As before, $\bar{\alpha}$ and β may be obtained from the boundary conditions $h(x_0) = h_0$ and $h(x_1) = h_1$.

Interestingly, by exploring mathematical analogies between beach profiles and relativistic cosmology—and assuming "deep water" (defined as $h \gg x$, that is, not in terms of wavelength)—Faraoni (2019) has recently derived a similar expression to equation (13), that is, with the exact same exponent.

Table 3
Ratio of the Functional $J[h(x)]$ Obtained by Equation (13) and a Linear Profile to That Obtained From the Measured Profiles, That is, Ratio of $J[h(x) = \text{Profile Shown in Left Column}]$ to $J[h(x) = \text{Measured Profile}]$

	Jenkins and Inman						Wang and Kraus		
	a	b	c	d	e	f	209	279	559
equation 13	0.89	1.06	0.89	0.75	1.01	0.86	1.05	0.99	0.80
linear profile	1.67	1.68	1.54	1.79	1.56	1.75	1.60	1.40	1.55

Note. Note that in all cases J[linear profile] > J[measured profile].

4.3. Comparison Against Field and Laboratory Data

In Figure 4, a good qualitative agreement is observed between equation (13) and six of the profiles employed for comparison; equation (13) replicates correctly the concave section near the breaking bar and the tendency toward a milder, uniform slope offshore. This good agreement is verified quantitatively for all profiles in Table 3, which gives the ratio of the functional $J[h(x)]$ (equation 4) yielded by the proposed profile to the functional obtained via the measured profile, that is, the ratio of $J[h(x) = \text{equation 13}]$ to $J[h(x) = \text{measured profile}]$. A linear profile is also included for reference. Note that in average a linear profile yields a functional (energy dissipation) approximately 40% larger than that of the measured profiles, whereas the functionals obtained from the proposed EBP formulation generally falls within about ± 10% of the latter.

4.4. The Influence of the Seaward Boundary

Strictly speaking, the seaward boundary of the profile (x_1, h_1) should be given by the point beyond which there is no morphodynamic interaction between the surface waves and the seabed, that is, the depth of closure. However, this depth is difficult to determine without a priori knowledge on the approaching waves (wave height and period) and sediment (see, e.g., Hallermeier, 1981;Kraus et al., 1998), and a significant degree of empiricism is typically involved in its identification. Therefore, for the purposes of this study, the seaward boundary could in principle be any point along the constant-slope, seaward part of the profile (i.e., where h'' vanishes). Nevertheless, different selections of the point (x_1, h_1) will naturally lead to different values of the constants $\bar{\alpha}$ and β in equation (13) (see section 3.1) and thus strictly different profiles. Figure 5 (left) explores the sensitivity of equation (13) to the selection of the boundary (x_1, h_1) for one profile, representative of all others. The effect of the seaward boundary is negligible in the vicinity of x_0 but becomes more evident as $x \to x_1$. In general, sensitivity to the seaward boundary is reduced for larger values of x_1, and so a "sufficiently far" seaward boundary should be selected, so long as the point lies on the constant-slope part of the profile. An alternative to this boundary condition (based on the value of h' at $x = x_0$) was also tested, with unsuccessful results, as discussed in section 5.

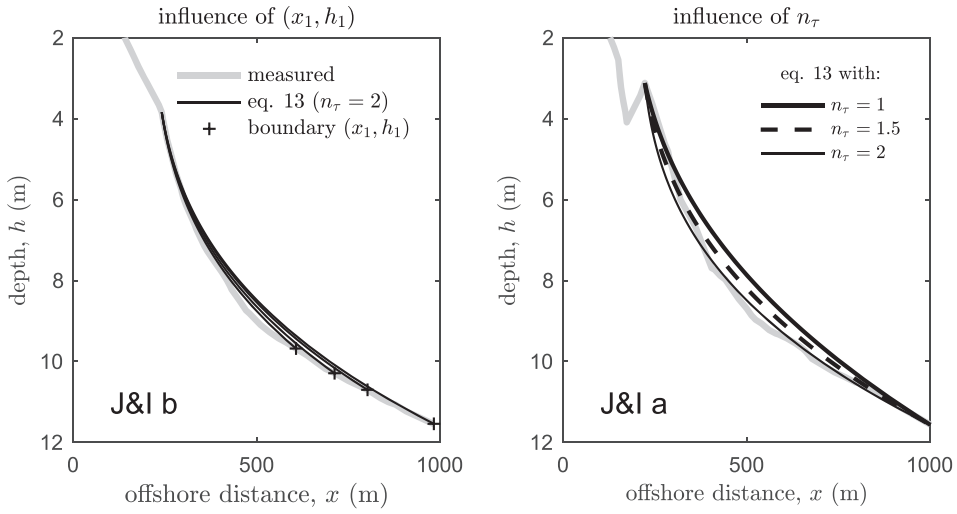

Figure 5. Left: Influence of the selection of the seaward boundary (x_1, h_1) on the profile predicted by equation (13) (for $n_\tau = 2$). Right: Effect of n_τ (from $|\tau_b| = K_\tau u_b^{n_\tau}$) on the profile predicted by equation (13). The measured profiles are J&I b and J&I a, respectively, which are representative of all other profiles considered.

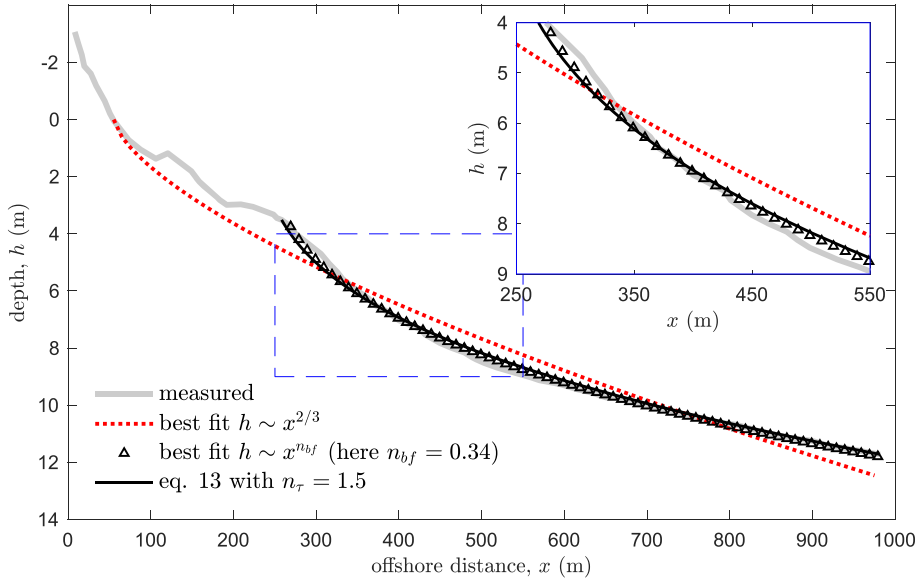

Figure 6. The theoretical profile proposed here (equation 13, using $n_\tau = 1.5$) is compared against a measured profile (in this case J&I c) and a best-fit power law curve of the form $h \sim x^{n_{bf}}$, where n_{bf} is one of the fitting parameters. The Dean profile ($h \sim x^{2/3}$) is added for reference.

4.5. The Influence of n_τ

Up to this point we have adopted $n_\tau = 2$ (i.e., $|\tau_b| = K_\tau u_b^2$). In Appendix A we look into the potential values that may be expected of n_τ in practice and conclude that this parameter should approximately lie in the range $1 \leq n_\tau \leq 2$, with the lower and upper limits corresponding to laminar and rough turbulent boundary layers, respectively. Note that the expected values of n_τ lead to the two limit cases $h \sim x^{2/5}$ and $h \sim x^{4/13}$. Figure 5 (right) illustrates the effect of n_τ on the profile predicted by equation (13) within the range $1 \leq n_\tau \leq 2$. As may be expected from inspection of the mathematical structure of equation (13), the effect of n_τ on the proposed profile is substancial since this parameter is part of the exponent to which h is raised. Moreover, the observed behavior of the proposed EBP for increaasing n_τ backs the energy minimization argument underpinning this work, namely, for larger values of n_τ, a profile tending to minimize energy dissipation will develop a more concave shape in order to increase h, which then reduces τ_b and hence $\bar{\epsilon}$ (see equation 1).

4.6. Comparison Against Best-Fit Power Law Curves

Power law curves of the form $h(x) = A_{bf}(x - b_{bf})^{n_{bf}}$, where the subscript "$bf$" denotes best-fitting parameters, have been fitted to each of the nine profiles considered. The values of n_{bf} obtained from the best fits fall in the range $[0.28, 0.38]$ ($[0.25, 0.41]$) for the J&I (W&K) profiles, confirming previous observations (e.g., Inman et al., 1993; Larson et al., 1999) that highlight the fact that the exponent in the power law curve, when applied to the shoaling part of the profile, is typically smaller than (the popular value) 2/3. In agreement with these insights, the two limit cases of the profile proposed here ($h \sim x^{2/5}$ and $h \sim x^{4/13}$) yield exponents in the range $[0.31, 0.40]$. Figure 6 illustrates the remarkably good agreement between the best fits (to profile J&I c) and the proposed theoretical profile (equation 13) for $n_\tau = 1.5$. The Dean profile (i.e., $h \sim x^{2/3}$) is included in Figure 6 just for reference, noting that its relatively poor predictive performance beyond the surf zone is well documented (see, e.g., Fredsøe & Deigaard, 1992; Larson et al., 1999).

5. Discussion

The theoretical EBP described by equation (13) represents an approximate solution to the problem of finding a function $h(x)$ that extremizes the functional in equation (4), subject to known boundary conditions $h(x_0)$ and $h(x_1)$, and the evidence-based conditions a–d described in section 2. It has been shown that this theoretical profile

1. agrees well with beach profiles measured in field and laboratory, particularly from a qualitative perspective: the predicted profile is concave near the wave breaking point and the bed slope tends to a smaller, constant value offshore (see Figures 2 to 6);
2. yields values of the functional $J[h(x)]$ (an indicator of the wave-average energy dissipation rate) which are close (generally within $\pm$ 10%) to those estimated from the measured profiles (see Table 3); and
3. recovers the popular power law relation between h and x, in turn, based on a large body of empirical observations, but where it is worth remarking that the predicted exponent (i.e., $4/[3n_\tau + 7]$) is not an arbitrarily free parameter. The exponent relates to the bed shear stress (which is responsible for the energy dissipation of nonbreaking, inviscid waves) via n_τ in $|\tau_b| = K_\tau |u_b|^{n_\tau}$, for which realistic values ($1 \leq n_\tau \leq 2$; see Appendix A) have been employed throughout this study. These values lead to the limit cases $h \sim x^{2/5}$ and $h \sim x^{4/13}$, in agreement with previous observations of profiles under nonbreaking waves (e.g., Inman et al., 1993).

The above remarks suggest that a principle of energy extremization may indeed underpin the particular shape adopted by equilibrium beach profiles under nonbreaking waves. However, next, we identify and discuss the main limitations of the mathematical treatment presented here, followed by further comments on other relevant aspects of this work.

A. All but one of the five key assumptions (1–5) invoked in section 2 refer to the geophysical properties of the site considered (all but Assumption 2; see below). These assumptions are rather restrictive and do not represent the complexity of real beach profiles, particularly those in field.
B. Assumption 2 in section 2 refers to the validity of linear wave theory. Although the robustness of this theory is well known, its validity is certainly questionable near the wave breaking point, where nonlinear effects become important (Thornton & Guza, 1983). Assumption 2 may also fail at deeper waters (near x_1), but this is expected to be less important since energy dissipation there is negligible.
C. The mathematical treatment presented here hinges on our ability to formulate the energy dissipation rate as some explicit function of the local water depth; in this case, $\bar{\epsilon} = K_\epsilon h^{-n_\epsilon}$ (equation 2). However, this is in general unlikely given that the friction factor f_f, embedded in K_ϵ, is typically defined so that it fits the curve $|\tau_b| \propto u_b^2$, with the consequence that empirically derived expressions for f_f are usually reported as intricate implicit equations (see Appendix A), the adoption of which would hinder the analytical procedures adopted throughout this work.
D. The assumptions referred to in Point (A) may be restrictive but not physically unrealistic. Nevertheless, in order to be able to express $\bar{\epsilon}$ as $\bar{\epsilon} = K_\epsilon h^{-n_\epsilon}$, it was further stated that due to simple shoaling, the cross-shore variation of the wave height follows $H \sim h^{-1/4}$. But this prediction is based on the conservation of the wave energy flux (see, e.g., Svendsen, 2006), which then contradicts the foundational proviso that energy is being dissipated. However, this apparently crucial contradiction may be partially remedied by invoking the supposition that energy dissipation across the profile is vanishingly small, which aligns with our purpose of finding a profile that minimizes this quantity. Moreover, the $H \sim h^{-1/4}$ assumption has been shown to predict well the wave height variation due to shoaling both in field and laboratory (Guza & Thornton, 1980; Thornton & Guza, 1983). This may explain why comparison between the theoretical and measured profiles generally yields a good agreement despite this fundamental inconsistency in the theory, but also why largest disagreements are to be found near the shoreward boundary x_0, where energy dissipation is larger than further offshore (and where the validity of linear wave theory becomes particularly questionable, as discussed above).

On the waves irregularity: The assumption of monochromatic waves of constant amplitude has been invoked to simplify derivations, but this proviso could potentially be relaxed provided all adequate modifications are made (e.g., use of H_{rms} rather than H as in Thornton & Guza, 1983 or Larson et al., 1999), without an anticipated major impact on the key predictions and conclusions here discussed. The latter statement is supported by the good agreement observed between the theory and field and laboratory data, despite the fact that in most of these measured profiles (with the exception of profile W&K 559) irregular waves were present. Note that irregular waves will not brake at a single point but rather within a region near x_0; but again, the theory presented here is expected to be particularly limited when $x \to x_0$, as discussed in points (B) and (D) above.

On the constraints imposed: Whereas the bed slope constraint (discussed below) is an uncontroversial requirement, constraints b–d discussed in section 2 may seem overrestrictive. These constraints are however necessary to ensure an adequate formulation of the problem leading to a realistic solution. For instance, bypassing the Euler-Lagrange equation, a solution to the variational problem may be proposed (by inspection of Figure 2) that complies with conditions a, b, and d, but not c, as shown in Figure 3 (red dotted line). However, this solution would have a very large second derivative where the slope changes and would exhibit an unrealistically high sensitivity to the selection of the seaward boundary (unlike the proposed profile). Constraint c is hence necessary (similar arguments may be made for the other constraints). EBPs in nature may not be strictly monotonic (see W&K 279 in Figure 4), which may be caused by complex phenomena not accounted for in this treatment (see Point (A) above); however, the smooth monotonic increase of depth is arguably a reasonable description of the shoaling part of most beach profiles (see any other figure in this paper).

On the incorporation of the bed slope constraint: The method employed to ensure compliance with the bed slope constraint (see section 4.2) is one of two alternatives tested by the author. Based on the a posteriori knowledge that maximum values of h' predicted by the solution are always found at $x = x_0$ (see, e.g., Figure 3), the other alternative (the unsuccessful results of which are not shown) consisted in imposing the boundary condition $h'(x = x_0) =$ some value $\leq \tan\phi$, which would then ensure that $h'(x) \leq \tan\phi$ for all $x \in [x_0, x_1]$. However, removing the seaward boundary condition $h(x_1) = h_1$ had the consequence of promoting a curve that would attain unrealistically large values of h in the domain in order to minimize the target functional (removing instead $h(x_0) = h_0$ led to similarly unrealistic results). This would in turn violate the implicit restriction that predicted values of $h(x)$ must be sufficiently small so that interaction between the surface waves and the bed is guaranteed. Note that this condition is naturally met by imposing the data-based boundary conditions $h(x_0) = h_0$ and $h(x_1) = h_1$. As discussed in section 4.2, the author is unaware of any methods to solve exactly the variational problem considered here via analytical means due to the nature of the angle of repose constraint (i.e., an inequality), but some ideas for future analytical or semi-analytical treatments may include the use of finite differences and minimizing sequences as in Courant and Hilbert (1953).

On the use of the derived EBP for practical purposes: As discussed in section 1, theoretical EBPs are often employed in reduced-order models with different predictive aims. However, it must be noted that the goal of this manuscript is not per se to derive and promote a predictive engineering tool (another EBP formulation) but rather to investigate the energy economy principle discussed throughout the manuscript. Therefore, a thorough validation of the expression derived (equation 13) against a large number of measured beach profiles is not a priority of this work. This, of course, does not preclude others from testing the predicitve capabilities of equation (13) in field and laboratory. To that end, however, it is reminded that (i) equation (13) is only valid for nonbreaking waves and (ii) suitable boundary conditions must be selected, for which it is anticipated that a certain degree of empiricism will be involved (see sections 3.1 and 4.4).

On the minimum versus maximum controversy: Whereas from a mathematical perspective there is little difference between the minima and maxima of a functional (they are both extrema), this is not true from a physical viewpoint. Thus, it is somewhat disturbing that different authors who arrive at equation (7) formulate the diametrically opposed claims that solution to this integral leads to *minimization* (this paper; Larson et al., 1999) or *maximization* (Jenkins & Inman, 2006) of wave energy dissipation $\mathcal{D}$ (equation 3). We argue that there is now sufficient evidence to state that the stationary value to which solution of equation (7) leads cannot be a maximum. This is succinctly illustrated in Figure 2 (right). What is more, that a linear profile (dotted line in Figure 2 left) always yields a larger value of the functional $J[h]$ than any measured profile (see Table 3 but also Maldonado & Uchasara, 2019) is further evidence that beach profiles do not tend to shapes that thereafter *maximize* the rate of energy dissipation; indeed, experiments on EBPs often set a linear profile, or plane beach, as the initial state from which the profile departs toward its typical concave shape (see, e.g., Dean, 1991). A mathematically rigorous proof of the above claim would involve estimation of the second variation of J, which is beyond the scope of the present work, and may not at all be possible: Faraoni (2019) shows that equation (7) may only be analytically extremized for physically meaningless (in the context of beach profiles) values of n_τ, such as $n_\tau < 0$. In short, EPBs under nonbreaking waves may or not tend to a form that strictly minimizes energy dissipation (see paragraph below), but at least we can be certain that they do not morph into equilibrium shapes that seek to thereafter maximize $\mathcal{D}$.

This paper represents a more comprehensive attempt (compared to previous works) at testing the hypothesis of EBPs under nonbreaking waves as systems that minimize energy dissipation, with results indicating that the hypothesis may be correct. However, as discussed in this section, significant simplifications have been made in the conceptualization of the problem, and the analytical solution to the constrained variational problem is only approximate. In future, more thorough tests of this hypothesis might include computational approaches to the optimization problem, semianalytical treatments, and ad hoc experiments. A future variational approach to this problem may include, not only the equilibrium (final) state of the profile, but also its initial configuration and all intermediate profiles, and account not only for the dissipation of wave energy but also the work required to reshape the profile and/or the potential energy contained in the sediment grains making up the shoreface (all subject to a realistic morphodynamic interaction, e.g., that respects the constraint imposed by the sediment threshold of motion). An approach of this sort might even reconcile the energy minimization hypothesis discussed here with the maximum entropy production viewpoint adopted by Jenkins and Inman (2006). It is hoped that this theory may also motivate similar investigations into other geomorphological features besides beach profiles.

6. Conclusions

After Larson et al. (1999), we enquire whether beach profiles under nonbreaking waves tend to an equilibrium shape that thereafter minimizes the rate of wave energy dissipation due to bed friction. Employing linear wave theory, a variational problem is formulated, which (unlike Larson et al., 1999) we attempt to solve directly via analytical means without a priori assumptions on the mathematical structure of the solution. We remark that for the solution to be realistic, the problem must consider additional constraints (e.g., related to the limitation imposed by the sediment's angle of repose). These constraints lead us to adopt an analytical solution to the optimization problem that is only approximate. Thus, the profile derived here (i.e., $h \sim x^{4/(3n_\tau+7)}$; see equation 13) may be understood as one that tends to minimize the energy dissipation of linear, nonbreaking waves while retaining realistic features. The profile recovers the well-known, empirical data-based power law relation between depth and cross-shore distance. However, it must be noted that the exponent in the power law function derived is not an arbitrarily free parameter (as in Larson et al., 1999); it depends on the degree of nonlinearity in the relation between the near-bed orbital velocity and the bed shear stress (the latter being the main mechanism by which nonbreaking waves dissipate energy), leading to the limit cases $h \sim x^{2/5}$ and $h \sim x^{4/13}$ for laminar and rough turbulent boundary layers, respectively. These limit cases (in particular, the values of the exponents) confirm insights from previous studies on beach profiles under nonbreaking waves. The good agreement between the theoretical profile proposed here and equilibrium beach profiles measured in field (Jenkins & Inman, 2006) and laboratory (Wang & Kraus, 2005) suggests that the energy minimization hypothesis posed by Larson et al. (1999) is correct. However, given the conceptual and methodological limitations of this work (discussed in section 5), this hypothesis requires further tests before definite conclusions can be drawn, perhaps employing both computational and experimental tools. We hope that the theory presented here will be useful to that end.

Appendix A: Expected Values of n_τ

The objective of this appendix is to estimate a range of expected values of n_τ in $|\tau_b| = K_\tau |u_b|^{n_\tau}$, where K_τ must be independent of both h and u_b.

The wave friction factor, f_f, is conventionally defined so that it fits the expression $\tau_{bo} = K_{\tau_2} u_{bo}^2$ (see, e.g., Svendsen, 2006), where f_f is embedded in K_{τ_2}, and τ_{bo} is the amplitude or maximum value of $\tau_b(t)$. This definition of f_f is in practice also extended to include the instantaneous bed shear stress $\tau_b(t) = K_{\tau_2} u_b(t)^2$, retaining K_{τ_2} as a constant (Svendsen, 2006); thus, $K_{\tau_2} = K_\tau$. The friction factor f_f may be empirically obtained as a function of the wave Reynolds number, Re, and relative roughness, r_e (see, e.g., Jonsson, 1967; Jonsson & Carlsen, 1976; Kamphuis, 1975), in turn defined as

$$\mathrm{Re} \equiv \frac{u_{bo}\zeta_b}{\nu} \quad \text{and} \quad r_e \equiv \frac{k_e}{\zeta_b}, \tag{A1}$$

where ζ_b is the wave horizontal excursion at the bed, ν is the water's kinematic viscosity, and k_e is a length characterizing the bed roughness. Let us now consider the two limit flow regimes: laminar and rough turbulent flows. Under the former (latter), f_f solely depends on Re (r_e), whereas in general $f_f = f(\mathrm{Re}, r_e)$. Based

on the defining expression for f_f, namely, $\tau_{bo} = K_{\tau_2} u_{bo}^2$, it can be shown (Dean & Dalrymple, 1991) that $f_f \sim \mathrm{Re}^{-1/2}$ in a laminar boundary layer. Moreover, we know that for shallow linear waves, $u_{bo} \sim h^{-3/4}$ and $\zeta_b \sim h^{-3/4}$ (see Appendix B), such that $\mathrm{Re} \sim h^{-3/2}$, which yields

$$\tau_{bo} \sim \mathrm{Re}^{-\frac{1}{2}} u_{bo}^2 \sim h^{-\frac{3}{2}\left(-\frac{1}{2}\right)} h^{-\frac{3}{4}(2)} \Rightarrow \tau_{bo} \sim h^{-\frac{3}{4}}. \tag{A2}$$

Thus, from $|\tau_b| = K_\tau |u_b|^{n_\tau} \sim h^{-\frac{3}{4} n_\tau}$ (see section 2), we get $n_\tau = 1$ for laminar flow. In rough turbulence, the relation $f_f = f_f(r_e)$ is found empirically. For instance, Kamphuis (1975) proposes $f_f \sim r_e^{0.75}$, while Soulsby (1997) suggests that $f_f \sim r_e^{0.52}$, and for Swart (1974) f_f is a constant (i.e., $f_f \sim r_e^0$). Since $r_e \sim \zeta_b^{-1} \sim h^{3/4}$, the aforementioned works yield, respectively, $f_f \sim h^{0.56}$, $f_f \sim h^{0.39}$, and $f_f \sim h^0$, which imply, according to $\tau_{bo} = K_{\tau_2} u_{bo}^2 \sim f_f h^{-3/2}$, that $\tau_{bo} \sim h^{-0.94}$, $\tau_{bo} \sim h^{-1.11}$, and $\tau_{bo} \sim h^{-1.5}$, and thus, $n_\tau = 1.25$, $n_\tau = 1.48$, and $n_\tau = 2$ for each of the works discussed. We can then expect n_τ, as defined in this work, to lie in the range $1 \leq n_\tau \leq 2$.

The above estimates of n_τ represent a crude approximation; in general, the empirically determined function $f_f = f(\mathrm{Re}, r_e)$ (often an implicit equation) may not allow f_f (and thus τ_b) to be expressed as a power law function of h, particularly not one with a constant exponent (see section 5).

Appendix B: Relations From Linear Wave Theory

For convenience, this appendix derives well-known relations used throughout the manuscript between relevant variables (u_{bo}, H, ζ_b) and h, based on the shallow water approximation of linear wave theory (see, e.g., Dean & Dalrymple, 1991; Svendsen, 2006). Variables not defined here are defined elsewhere in the paper. Near the bed ($z \to -h$), the magnitude of the horizontal particle velocity and displacement predicted by linear wave theory are $u_{bo} = (H/2)\omega(1/\sinh kh)$ and $\zeta_b = (H/2)(1/\sinh kh)$, respectively, where ω is the angular frequency, $k = 2\pi/\lambda$ is the wavenumber, and λ is the wavelength. The shallow water approximation, valid when $\lambda \gg h$, implies that $\sinh kh \to kh$ and $\omega/k \to \sqrt{gh}$ (where g is the gravitational acceleration), thus leading to $kh = \omega\sqrt{h}/\sqrt{g}$ and hence

$$u_{bo} = \frac{H}{2}\sqrt{\frac{g}{h}} \quad \text{and} \quad \zeta_b = \frac{H}{2\omega}\sqrt{\frac{g}{h}}. \tag{B1}$$

Incorporation of simple shoaling, in shallow water, gives the variation of H across the profile as the ratio to the approach wave height in deep water, H_∞, namely,

$$\frac{H}{H_\infty} = \frac{1}{\sqrt{2\omega}}\left(\frac{g}{h}\right)^{\frac{1}{4}} \Rightarrow H \sim h^{-1/4}. \tag{B2}$$

The above equation can then be used in equation (B1) to yield:

$$u_{bo} = \frac{1}{2}\left(\frac{H_\infty}{\sqrt{2\omega}}\right)\left(\frac{g}{h}\right)^{\frac{3}{4}} \Rightarrow u_{bo} \sim h^{-\frac{3}{4}} \tag{B3}$$

and

$$\zeta_b = \frac{1}{2\omega}\left(\frac{H_\infty}{\sqrt{2\omega}}\right)\left(\frac{g}{h}\right)^{\frac{3}{4}} \Rightarrow \zeta_b \sim h^{-\frac{3}{4}}. \tag{B4}$$

Appendix C: Alternative Solution by Series Expansion

The integral in equation (7) may also be solved by first expanding the integrand in Taylor series. It is pertinent to do so around h_0, given that most energy dissipation takes place in shallow regions of the profile. The solution thus obtained presents a similar behavior to equation (11), and as expected, both solutions agree for increasing order of the expressions (although the series expansion solution converges significantly more slowly), as illustrated in Figure C1 (left). The procedure described in section 4.2 may then be applied to this alternative solution, namely, highest-order terms can be discarded until the condition $|h'(x)| \leq \tan\phi$

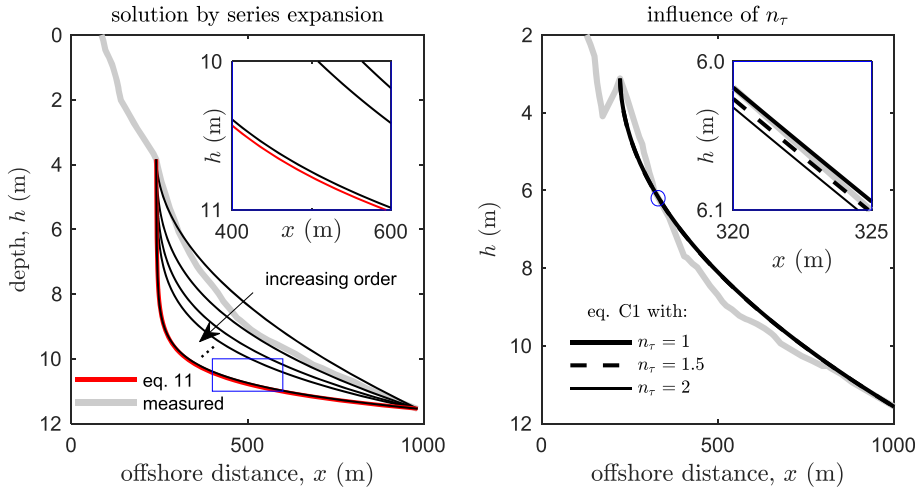

Figure C1. Left: Behavior of the solution to the integral in equation (7) by series expansion for increasing degree of the polynomial (black lines); curves are shown for Degrees 2, 3, 4, 5, and 11. The polynomial of Degree 11 agrees well with equation (11) with four terms retained (red line). For all curves $n_\tau = 2$. Right: Influence of n_τ on the profile predicted by equation (C1). The measured profiles are J&I b (left) and J&I a (right).

is satisfied for all $x \in [x_0, x_1]$. The polynomial that complies with the bed slope constraint is quadratic in h, namely,

$$x(h) = \sqrt{\frac{\hat{\alpha} h_0^m}{1 - \hat{\alpha} h_0^m}}\, h + \frac{m\sqrt{\hat{\alpha} h_0^m}}{4h_0(1 - \hat{\alpha} h_0^m)^{3/2}}(h - h_0)^2 + \hat{\beta}, \tag{C1}$$

where as with equation (13), values of $\hat{\alpha}$ and $\hat{\beta}$ are determined from the boundary conditions via solution of the associated system of two nonlinear equations (but note that $\hat{\alpha}$ and $\hat{\beta}$ need not evaluate to the same values as $\bar{\alpha}$ and β in equation 13 for the same boundary conditions). Equation (C1) also yields a good qualitative agreement when compared against field and laboratory data (see Figure 4). Values of the functional J yielded by equation (C1) are similar to those arising from equation (13) (see supporting information), and just as the latter, equation (C1) is relatively insensitive to the somewhat arbitrary selection of the seaward boundary (x_1, h_1) (not shown here). However, equation (C1) is virtually insensitive to n_τ, as shown in Figure C1 (right). This rigidity in the solution is a consequence of the mathematical structure of the Taylor series and is a weakness of the expression from the perspective of physical meaningfulness: Equation (C1) predicts that both turbulent and laminar boundary layers lead to essentially the same profile. For this reason we relegate equation (C1) to this appendix as another approximate solution to the variational problem considered here, which has been tested and shown to be inferior to equation (13).

Acknowledgments
The author wishes to thank: Professor P. Wang for kindly providing the data in Wang and Kraus (2005) and M. Uchasara for carefully digitizing that in Jenkins and Inman (2006); Dr J. A. Zielińska for repeated proofreading and helpful feedback; Dr J. Arriaga for flagging a paper that would eventually lead to this publication and two anonymous reviewers and the associate editor, whose insightful comments have led to a significantly improved version of this manuscript. Codes employed in this paper as well as the supporting information can be downloaded from https://doi.org/10.5281/zenodo.3725621 and https://doi.org/10.5281/zenodo.3725639, respectively. This research was not funded.

References

Ashton, A. D., & Murray, A. B. (2006). High-angle wave instability and emergent shoreline shapes: 1. Modeling of sand waves, flying spits, and capes. *Journal of Geophysical Research*, *111*, F04011. https://doi.org/10.1029/2005JF000422

Bowen, A. J. (1980). Simple models of nearshore sedimentation: Beach profiles and long-shore bars. In S. B. McCann (Ed.), *The coastaline of canada: Littoral processes and shore morphology* (pp. 1–11). Halifax, Nova Scotia: Geological Survey of Canada.

Bronshtein, I. N., Semendyayev, K. A., Musiol, G., & Muehlig, H. (2007). *Handbook of mathematics* (5th ed.). Berlin: Springer.

Brunn, P. (1954). *Coast erosion and the development of beach profiles* (Tech. Memo No. 44). US Army Corps of Engineers.

Chen, S., Gibbons, G. W., & Yang, Y. (2015). Friedmann-Lemaitre cosmologies via roulettes and other analytic methods. *Journal of Cosmology and Astroparticle Physics*, *2015*(10), 56.

Cline, D. (2017). *Variational principles in classical mechanics*. Rochester, NY: University of Rochester.

Courant, R., & Hilbert, D. (1953). *Methods of mathematical physics* (1st1st ed., Vol. I). U.S.A.: Interscience Publishers.

Dean, R. G. (1977). *Equilibrium beach profiles: US Atlantic and Gulf coasts* (Ocean Engineering Report No. 12). Newark, Delaware: University of Delaware.

Dean, R. G. (1991). Equilibrium beach profiles: Characteristics and applications. *Journal of Coastal Research*, *7*, 53–84.

Dean, R. G. (2003). *Beach nourishment: Theory and practice* (Vol. 18). Singapore: World Scientific Publishing Company.

Dean, R. G., & Dalrymple, R. A. (1991). *Water wave mechanics for engineers and scientists* (Vol. 2). Singapore: World Scientific Publishing Company.

Dean, R. G., & Houston, J. R. (2016). Determining shoreline response to sea level rise. *Coastal Engineering*, *114*, 1–8.

Dong, P. (2008). Long-term equilibrium beach profile based on maximum information entropy concept. *Journal of Waterway, Port, Coastal, and Ocean Engineering*, *134*(3), 160–165.

Falqués, A., & Calvete, D. (2005). Large-scale dynamics of sandy coastlines: Diffusivity and instability. *Journal of Geophysical Research*, *110*, C03007. https://doi.org/10.1029/2004JC002587

Faraoni, V. (2019). Analogy between equilibrium beach profiles and closed universes. *Physical Review Research*, *1*(3), 33002.

Fredsøe, J., & Deigaard, R. (1992). *Mechanics of coastal sediment transport, Advanced series on ocean engineering* (Vol. 3). Singapore: World Scientific.

Guannel, G., Ruggiero, P., Faries, J., Arkema, K., Pinsky, M., Gelfenbaum, G., et al. (2015). Integrated modeling framework to quantify the coastal protection services supplied by vegetation. *Journal of Geophysical Research: Oceans*, *120*, 324–345. https://doi.org/10.1002/2014JC009821

Guza, R., & Thornton, E. B. (1980). Local and shoaled comparisons of sea surface elevations, pressures, and velocities. *Journal of Geophysical Research*, *85*(C3), 1524–1530.

Hallermeier, R. J. (1981). A profile zonation for seasonal sand beaches from wave climate. *Coastal Engineering*, *4*, 253–277.

Inman, D. L., Elwany, M. H. S., & Jenkins, S. A. (1993). Shorerise and bar-berm profiles on ocean beaches. *Journal of Geophysical Research*, *98*(C10), 18181.

Jara, M., González, M., & Medina, R. (2015). Shoreline evolution model from a dynamic equilibrium beach profile. *Coastal Engineering*, *99*, 1–14.

Jenkins, S. A., & Inman, D. L. (2006). Thermodynamic solutions for equilibrium beach profiles. *Journal of Geophysical Research*, *111*, C02003. https://doi.org/10.1029/2005JC002899

Jonsson, I. G. (1967). Wave boundary layers and friction factors. In *Coastal engineering 1966* (pp. 127–148). Tokyo, Japan: American Society of Civil Engineers in New York, N.Y.

Jonsson, I. G., & Carlsen, N. A. (1976). Experimental and theoretical investigations in an oscillatory turbulent boundary layer. *Journal of Hydraulic Research*, *14*(1), 45–60.

Kamphuis, J. W. (1975). Friction factor under oscillatory waves. *Journal of the Waterways, Harbors and Coastal Engineering Division*, *101*(2), 135–144.

Kraus, N. C., Larson, M., & Wise, R. A. (1998). Depth of closure in beach-fill design (Technical note No. ADA578584). Vicksburg, Mississippi: US army engineer waterways experiment station, coastal and hydraulics laboratory.

Larson, M., Kraus, N. C., & Wise, R. A. (1999). Equilibrium beach profiles under breaking and non-breaking waves. *Coastal Engineering*, *36*(1), 59–85.

Maldonado, S., & Uchasara, M. (2019). On the thermodynamics-based equilibrium beach profile derived by Jenkins and Inman. (arXiv:1908.07825[physics.geo-ph]).

Soulsby, R. (1997). *Dynamics of marine sands: A manual for practical applications*. London: Thomas Telford.

Svendsen, I. A. (2006). *Introduction to nearshore hydrodynamics* (Vol. 24). Singapore: World Scientific.

Swart, D. H. (1974). *Offshore sediment transport and equilibrium beach profiles* (Tech. Rep. No. 131). Delft Hydraulics Laboratory.

Thornton, E. B., & Guza, R. T. (1983). Transformation of wave height distribution. *Journal of Geophysical Research*, *88*(C10), 5925.

Wang, P., & Kraus, N. C. (2005). Beach profile equilibrium and patterns of wave decay and energy dissipation across the surf zone elucidated in a large-scale laboratory experiment. *Journal of Coastal Research*, *21*, 522–534.